Second-order model of entrainment in planar turbulent jets at low Reynolds number

S. Paillat and E. Kaminski

Citation: Physics of Fluids (1994-present) **26**, 045110 (2014); doi: 10.1063/1.4871521
View online: http://dx.doi.org/10.1063/1.4871521
View Table of Contents: http://scitation.aip.org/content/aip/journal/pof2/26/4?ver=pdfcov
Published by the AIP Publishing

PHYSICS OF FLUIDS **26**, 045110 (2014)

Second-order model of entrainment in planar turbulent jets at low Reynolds number

S. Paillat[a] and E. Kaminski
Institut de Physique du Globe de Paris, Sorbonne Paris Cité, Univ Paris Diderot, CNRS, 1 rue Jussieu, F-75252 Paris, France

(Received 5 December 2013; accepted 5 April 2014; published online 24 April 2014)

Turbulent jets and plumes are commonly encountered in natural and industrial environments, and have been the objects of seminal works on turbulent free shear flows. The dynamics of turbulent jets is most often described as a function of the so-called entrainment coefficient, α, which quantifies the entrainment of ambient fluid into the jets. This key parameter has been determined in numerous and extensive experimental, numerical, and theoretical studies of axisymmetric jets. However, data remain scarce on turbulent planar jets. Available studies have shown that at low distance from the source, α increases with the source Reynolds number, and that α increases with distance from the source for large source Reynolds number. But no link has been made between these two kinds of observation so far. To study the relative influence of source Reynolds number, Re_0, and distance from source on entrainment in planar turbulent jets, we perform new experiments at low Re_0 (between 59 and 424) with three different aspect ratio (185, 370, and 925) and at small and large distances from the source. Our experimental results show no systematic variations of α as a function of Re_0 or as a function of the distance from the source. To interpret these observations, we develop a formalism based on the flow velocity profiles, which yields an expression of α as a function of the evolution of the Reynolds shear stress and of the turbulent fluctuations of the radial and vertical velocities. We obtain that the main contribution to entrainment is related to the turbulent shear stress, and that second-order fluctuations of the velocity account for the observed variations of α. The evolution to a fully self-similar regime in which these fluctuations are fully negligible is too slow at small Re_0 for this regime to be observed in our experiments, even at the largest distances from the source. © *2014 AIP Publishing LLC*. [http://dx.doi.org/10.1063/1.4871521]

I. INTRODUCTION

The dynamics of turbulent jets and plumes depends on their source conditions and on the efficiency of turbulent entrainment of the surrounding fluid into the mean flow. Quantifying turbulent entrainment is key in assessing the rate of dilution and the rising height of natural and industrial jets and plumes. In volcanology, for example, entrainment plays an important role in the evolution of the eruptive column, and controls both the production of pyroclastic flows on the ground and the rate and the height of injection of volcanic gas and ash in the atmosphere.[1,2]

A large body of experimental and theoretical works on axisymmetric turbulent jets and plumes is available in the literature. In their seminal paper, Morton *et al.*[3] introduced the concept of entrainment coefficient, defined as the ratio of the lateral velocity of fluids engulfed in the flow to the vertical mean flow velocity. The values of the so-called "Gaussian" entrainment coefficient, α_G, are obtained by measuring the vertical velocity and fitting it by Gaussian functions. Such measurements in axisymmetric jets and plumes[4] have shown that entrainment is enhanced by positive buoyancy in plumes.[5,6] Recently, Carazzo and co-workers[7,8] proposed a theoretical expression of α_G that depends

[a]Author to whom correspondence should be addressed. Electronic mail: paillat@ipgp.fr

both on buoyancy (either positive or negative) and on the distance from the source. Their formalism accounts well for experimental measurements and observations on jets, plumes, and fountains,[9,10] and has been applied successfully to immiscible fluids[11] and reactive flows.[12]

Planar turbulent jets and plumes occurred also often in nature, for example, in the case of basaltic fissure eruptions, on Earth[13,14] and on other planets,[15] or in the case of the discharge of rivers into quiescent water.[16] However, they have not been the subject of as numerous and comprehensive studies as axisymmetric jets and plumes. For example, in their review, Fischer *et al.*[17] gave $\alpha_G = 0.035 \pm 0.001$ for pure planar jets and $\alpha_G = 0.070 \pm 0.001$ for pure planar plumes, but no models have been proposed so far to explain these values. Furthermore, to our knowledge, no experiments have been performed on planar negatively buoyant plumes yet. Our general goal is to provide a theoretical framework able to account for the effect of buoyancy and of potential self-similarity drift in planar jets and plumes, and to apply it to the modelling of geological turbulent flows. As a first step, we focus here on the behaviour of pure jets (i.e., driven only by their initial momentum, and without buoyancy forces).

The majority of experimental constraints on the entrainment coefficient in turbulent planar jets have been obtained at small and intermediate distances from the source ($5 < z/d < 150$, where z is the vertical distance from the source and d the source width). Determinations of α_G relied first on the measurement of opening angle of the jets from velocity profiles obtained by hot-wire anemometry.[18–21] Kotsovinos[22] and Ramaprian and Chandrasekhara[23] later obtained complementary data using Laser Doppler Anemometry. All these studies, performed at source Reynolds number, Re_0, larger than 1000 yielded a similar average value of $\alpha_G \approx 0.03$. However, from a detailed review of the literature, Kotsovinos[24] rather concluded that α_G was a function of distance from the source up to $z/d \approx 200$, where it reached a constant value $\alpha_G = 0.042$.

More recently, Namer and Ötüngen,[25] Suresh *et al.*,[26] and Deo[27] measured the opening angle of jets for various Re_0. They found that the value of α_G varied from 0.072 for $Re_0 \approx 250$, to 0.024 for $Re_0 > 6000$. Deo[27] experimentally studied the influence of the aspect ratio (width/length) of the source on α_G. At $Re_0 = 16\,000$, he showed that the entrainment coefficient varies between 0.016, for an aspect ratio of 20, to 0.032 for an aspect ratio of 72, which is consistent with the value of α_G given in the literature for higher aspect ratios and states that the entrainment coefficient does not depend on this parameter for such high aspect ratio.

In order to understand better the relative influence of this jet Reynolds number and distance from the source on the rate of entrainment in turbulent planar jets, we performed new experiments at small and large distances from the source, ranging from $z/d = 40$ to $z/d = 1000$, and at small source Reynolds numbers, ranging from $Re_0 = 60$ to $Re_0 = 420$. To interpret our experimental results as well as those from the literature in a common framework, we developed an expression for the entrainment coefficient derived from the theory of Priestley and Ball[28] and Kaminski *et al.*[7] for axisymmetric jets and plumes. Our results emphasize the key role played by the turbulent Reynolds stress on entrainment, and imply that second order refinements are required to explain the values of α_G measured at low Re_0 (<500). We propose that these second-order contributions can be calculated from the axial terms of the Reynolds stress which are often negligible in 2D turbulent jets.

II. ENTRAINMENT COEFFICIENTS IN PLANAR TURBULENT JETS

A. Review of literature data

Planar "pure" jets are turbulent free shear flows produced by a linear source of momentum infinite in one direction. They have no density anomaly relative to the ambient fluid, hence they are driven by their momentum flux only and no buoyancy forces are at play. The flow is bi-dimensional and can be described in a (x, z) plan, where z is the vertical direction, and x lies in the horizontal plane and is normal to the direction of the linear source, y.

Entrainment in turbulent planar jets and plumes is measured from the evolution of the vertical velocity profile in the flow as a function of z the vertical distance from the source. Previous studies have shown that the velocity $w(x, z)$ at distances from the source $z > 5d$ (with d the source width),

is well described by a Gaussian function,

$$w(x,z) = w_m(z)\exp\left(-\left[\frac{x}{b_w(z)}\right]^2\right), \tag{1}$$

where b_w is the $(1/e)$-width of the profile, and w_m is the velocity on the jet axis ($x = 0$). Following the approach of Morton *et al.*,[3] the mass and momentum conservation equations in pure planar jets are written as

$$\frac{\mathrm{d}}{\mathrm{d}z}(b_w w_m) = 2\,\alpha_G\, w_m, \tag{2}$$

$$\frac{\mathrm{d}}{\mathrm{d}z}\left(b_w w_m^2\right) = 0, \tag{3}$$

with α_G the "Gaussian" entrainment coefficient. The solutions of these equations are

$$b_w = b_{w_0} + 4\,\alpha_G\, z, \tag{4}$$

$$w_m = w_{m_0}/\sqrt{1 + 4\,\alpha_G\, z/b_{w_0}}, \tag{5}$$

with b_{w_0} and w_{m_0} values at the source ($z = 0$). From these expressions, the entrainment coefficient is determined locally as

$$\alpha_G = \frac{1}{4}\frac{\mathrm{d}b_w}{\mathrm{d}z}. \tag{6}$$

We report in Table I values of the entrainment coefficient computed from the plot of b_w against z^*. The data show that, for source Reynolds number, Re_0, higher that 3000, the entrainment coefficient displays a rather well-defined average value of 0.030 ± 0.006. The data are more variable at lower source Reynolds numbers, and α_G tends to increase when Re_0 decreases, up to $\alpha_G = 0.072 \pm 0.006$ for $Re_0 = 250$. This conclusion may seem at odds with the intuitive idea that entrainment should increase with increasing turbulence intensity, and could also be related to an evolution of self-similarity in the flow as a function of both Re_0 and distance from the source. To test this hypothesis, we performed experiments at low Re_0 (<500) and at small and large distances from the source.

B. Experimental measurements of the entrainment coefficient

In our experiments, turbulent linear jets are generated by the injection of fresh water through a line source in a $45 \times 30 \times 30$ cm^3 glass tank filled with fresh water (Figure 1) through eight small pipes to ensure a homogeneous supplying of the slot. To study the flow at large distances from the source, we use a slot width d of 0.2 mm (with an aspect ratio of 925) allowing measurements within a range of dimensionless distances relative to the source, $z^* = z/d$, between 200 and 800. To characterize the flow at smaller dimensionless distances from the source, we use slot widths of 1 mm (with an aspect ratio of 185) and 0.5 mm (aspect ratio of 370) and performed measurements in the range $40 < z^* < 150$ ($d = 1$ mm) and $80 < z^* < 250$ ($d = 0.5$ mm). The aspect ratio is always high enough not to influence the measurement of α_G.[27] In the three cases, we use flow rates Q between 0.5 and 5 l min^{-1}, which correspond to source Reynolds numbers between 50 and 450. For PIV measurements, the fluid is seeded with glass hollow sphere particles (LaVision 110P8) with a mean diameter of 11.7 μm and a median of 8 μm. Videos of the jets are recorded with a camera at a frame rate of 40 Hz with 2000 frames (it has been checked from longer recording and ensures the convergence of the measures), and Davis™ software is used to compute the instantaneous velocity in the flow by standard PIV methods. We use an interrogation window of 16×16 pixel with an elliptic weighting 4:1 and an overlap of 50% for the calculations of the correlations. We then calculate both the Reynolds-averaged velocities and their turbulent fluctuations using MATLAB™ programs.

Figure 2 shows pictures of turbulent jets at similar Re_0 but for two different slot widths, hence at two different distances from the source. The pictures show two different types of evolution of turbulence: (a), corresponding to small z^*, shows some meandering, whereas turbulence appears more regular in (b). Hence entrainment is likely to be different in the two cases.

TABLE I. Literature values of the "Gaussian" entrainment coefficient in planar turbulent jets, α_G calculated from the evolution of b_w with the distance from the source. The uncertainties are given by the standard deviation corresponding to the 95% confidence interval. Two different measurement methods were used: Hot-Wire anemometry (HWA), and Laser Doppler Anemometry (LDA). The dimensionless distance from the source is $z^* = \frac{z}{d}$, with d the width of the linear source. Re_0 is the Reynolds number at the source ($z^* = 0$).

Method	Fluid	Re_0	z^*	α_G	Ref.
HWA	Air	17 800	5–40	0.029 ± 0.006	18
HWA	Air	30 000	13.9–68.5	0.033 ± 0.003	19
HWA	Air	34 000	47–155	0.033 ± 0.003	20
LDA	Water	1700–1900	20.8–93.8	0.033 ± 0.008	22
HWA	Air	30 000	65–118	0.033 ± 0.004	21
LDA	Water	1500	10–60	0.034 ± 0.006	23
LDA	Water	2635–5197	45–80	0.036 ± 0.005	29
HWA/LDA	Air	1000	16–95	0.054 ± 0.002	25
HWA/LDA	Air	2000	16–95	0.037 ± 0.002	
HWA/LDA	Air	6000	16–95	0.030 ± 0.002	
HWA	Air	1500	0–100	0.041 ± 0.002	30
HWA	Air	3000	0–100	0.038 ± 0.002	
HWA	Air	7000	0–100	0.032 ± 0.002	
HWA	Air	10 000	0–100	0.029 ± 0.002	
HWA	Air	16 500	0–100	0.026 ± 0.002	
HWA	Air	250	20–100	0.072 ± 0.006	26
HWA	Air	550	20–100	0.064 ± 0.006	
HWA	Air	1100	20–100	0.060 ± 0.006	
HWA	Air	2000	20–100	0.044 ± 0.006	
HWA	Air	4000	20–100	0.032 ± 0.006	
HWA	Air	6250	20–100	0.025 ± 0.006	

With the maximum frame rate used in the experiments, we cannot measure the velocity in the near-source region with a satisfying accuracy. We determine the range of z^* where the measurements of velocity is correct by plotting the momentum flux $M = b_w w_m^2$ which should be constant in a pure jet against z^*. We then measure b_w and w_m, the 1/e-width and the centerline velocity of the Gaussian fits (Figure 3) in the range of constant M which are plotted in Figure 4. The entrainment coefficient α_G is deduced from these plots and shown in Table II as a function of the source conditions and distance from source.

Our results are quite variable and do not show any systematic variation of α_G as a function of Re_0. Furthermore, the maximal value we found for α_G is 0.046, whereas Suresh *et al.*[26] obtained $\alpha_G = 0.072$ for similar Re_0. Our values are more consistent with the ones obtained for $Re_0 > 1500$ in the literature (α_G between 0.029 and 0.045) and tend to be close to the highest values reported in these studies. To develop a quantitative interpretation of these results, we now follow the approach of Kaminski *et al.*[7] to derive an explicit expression of α_G as a function of the velocity and turbulent stress profiles.

III. THEORETICAL MODEL OF ENTRAINMENT IN PLANAR JETS

A. An explicit expression for the Gaussian entrainment coefficient α_G

Following Priestley and Ball,[28] we introduce $u = \overline{u} + u'$ the velocity along the x-direction and $w = \overline{w} + w'$ the velocity along the z-direction, with $\overline{u}$ and $\overline{w}$ their Reynolds time-averages, and u' and w' their turbulent fluctuations. At large Reynolds numbers, the time-averaged local mass and momentum conservation equations are written as

$$\frac{\partial \overline{u}}{\partial x} + \frac{\partial \overline{w}}{\partial z} = 0, \tag{7}$$

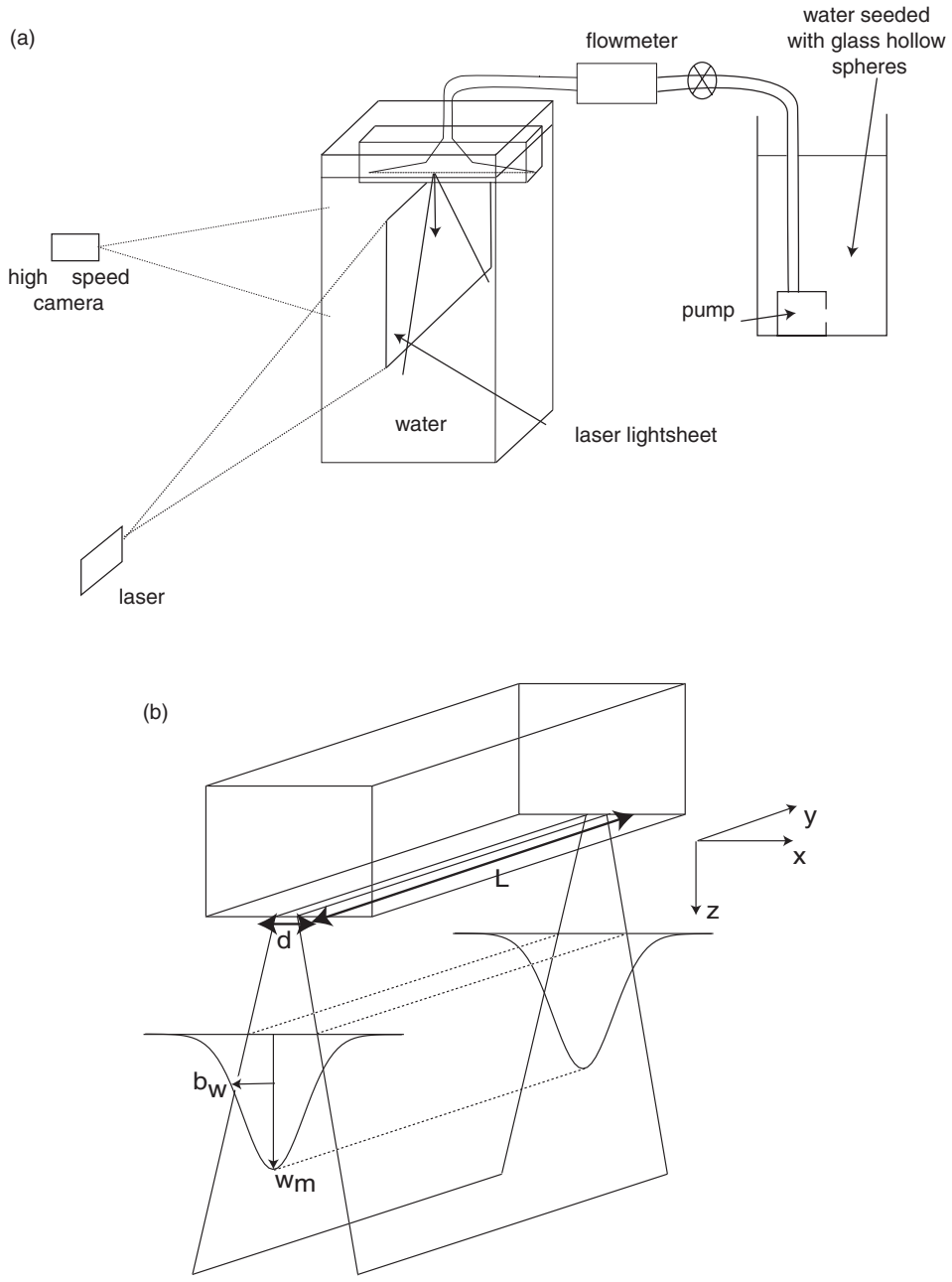

FIG. 1. (a) Overview of the experimental set-up. The jet is produced by a line source injecting fresh water, seeded with small glass particles, into fresh water at rest. A plane laser light sheet illuminates the flow which is recorded with a camera. Images are then correlated using DAVIS^{TM} software to obtain the velocity field. (b) Schematic representation of the flow.

$$\overline{u}\frac{\partial \overline{w}}{\partial x} + \overline{w}\frac{\partial \overline{w}}{\partial z} = \frac{1}{\rho}\frac{\partial \tau}{\partial x}, \tag{8}$$

where $\tau = -\rho\overline{u'w'}$ is the turbulent shear stress which accounts for entrainment,[28] and ρ is the fluid density. We combine the mass and momentum equations to rewrite the momentum equation as

$$\frac{\partial \overline{u}\,\overline{w}}{\partial x} + \frac{\partial \overline{w}^2}{\partial z} = \frac{1}{\rho}\frac{\partial \tau}{\partial x}, \tag{9}$$

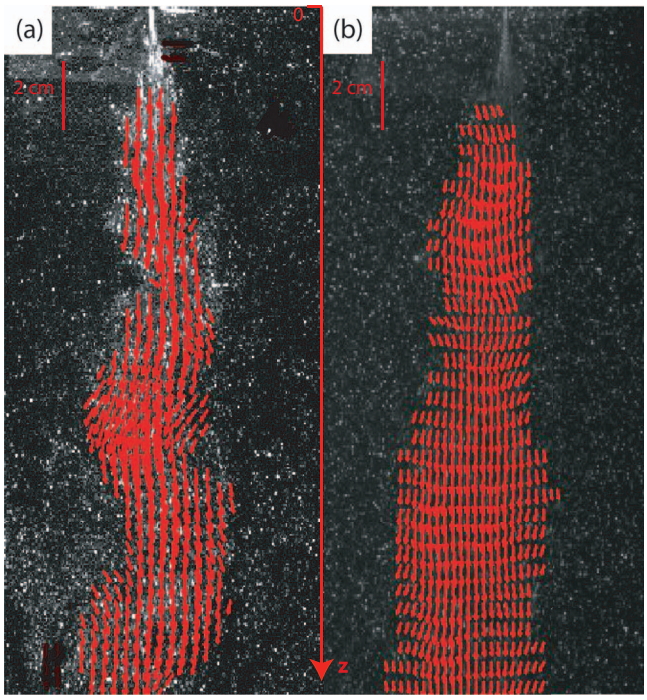

FIG. 2. Pictures of experimental turbulent jets at different distances from the source showing the velocity field determined by PIV (small red arrows: 3 cm = 1 m s^{-1}). (a) $Re_0 = 140$, $d = 1$ mm, $z^* = 20 - 200$; (b) $Re_0 = 156$, $d = 0.2$ mm, $z^* = 100$–1000. Although the Re_0 source numbers are similar in the two cases, the development of turbulence, hence of entrainment, appears quite variable, which suggests an effect of the distance from the source.

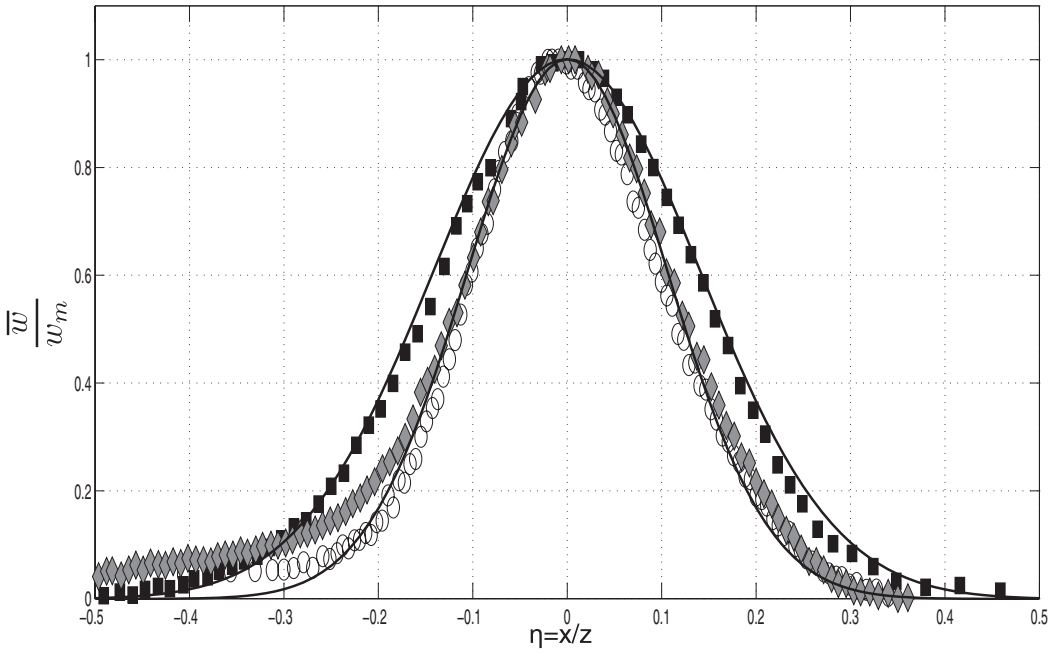

FIG. 3. Average velocity profiles over z^* for three experiments: HZ-3 (black squares), IZ-3 (gray diamonds), and LZ-2 (white circles).

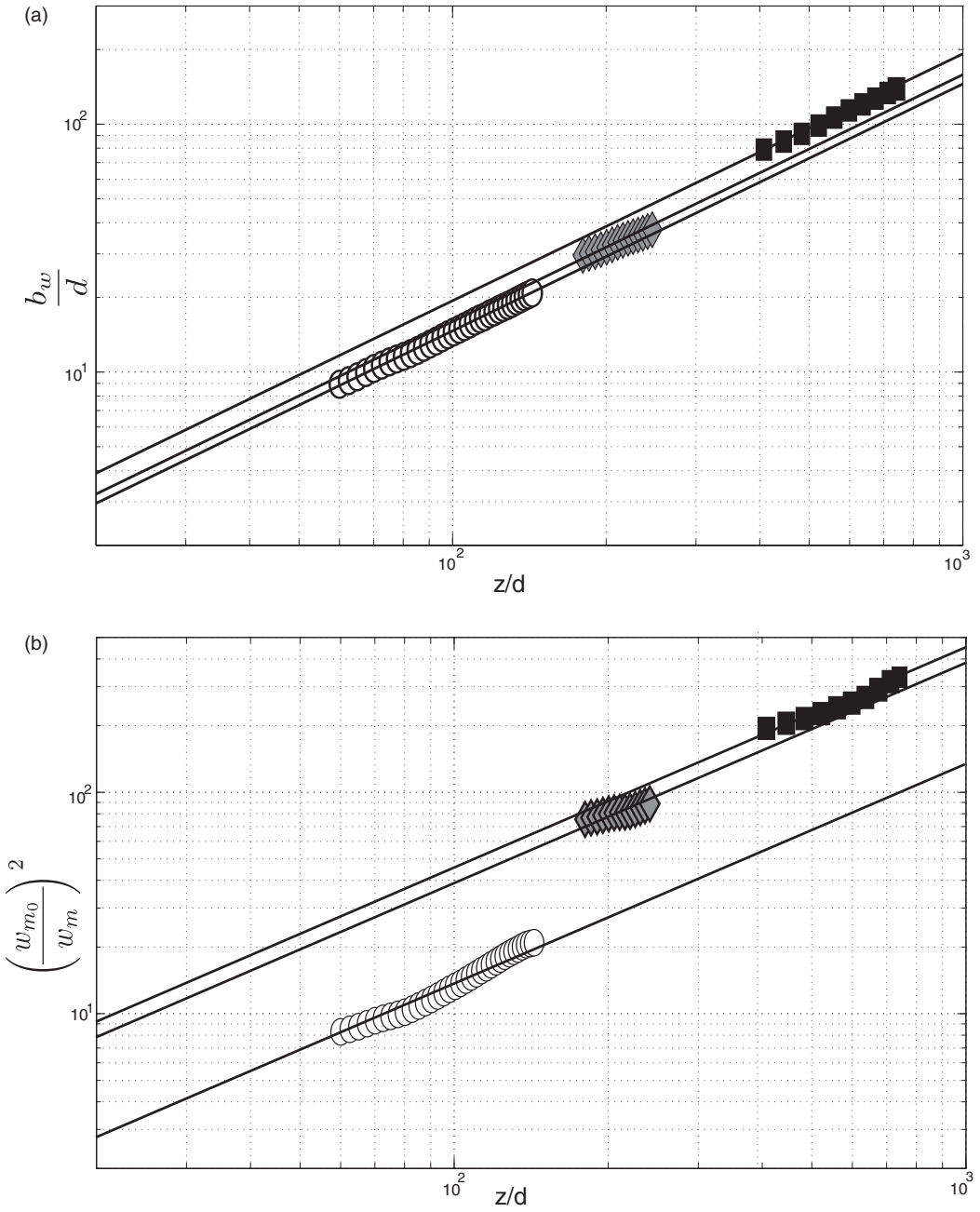

FIG. 4. Evolution of the half-width b_w (a) and the centerline velocity (b) of velocity profiles with z/d for all the experiments of Table II: HZ-3 (black squares), IZ-3 (gray diamonds), and LZ-2 (white circles).

and we integrate the mass and momentum conservation equations (7) and (9) subject to $u(x=0,z) = \tau(x=0,z) = \lim_{x\to\infty,z}\tau(x,z) = \lim_{x\to\infty,z} w(x,z) = 0$, which yields

$$\frac{\mathrm{d}}{\mathrm{d}z}Q(z) = -2\lim_{x\to+\infty}\overline{u}, \tag{10}$$

$$\frac{\mathrm{d}}{\mathrm{d}z}M(z) = 0, \tag{11}$$

TABLE II. Experimental results and source conditions.

Expt.	d (mm)	z^*	Q_0 (l min^{-1})	Re_0	α_G
HZ-1	0.2	400−600	0.69	62	0.037 ± 0.002
HZ-2	0.2	400−900	0.65	59	0.042 ± 0.008
HZ-3	0.2	400−750	1.47	133	0.043 ± 0.005
HZ-4	0.2	400−600	1.73	156	0.039 ± 0.004
HZ-5	0.2	450−750	2.41	217	0.034 ± 0.001
IZ-1	0.5	100−220	0.5	45	0.045 ± 0.004
IZ-2	0.5	170−240	0.97	87	0.037 ± 0.002
IZ-3	0.5	180−240	1.65	149	0.032 ± 0.003
IZ-4	0.5	140−220	4.22	381	0.031 ± 0.003
LZ-1	1	40−140	1.12	101	0.046 ± 0.004
LZ-2	1	60−140	1.52	137	0.036 ± 0.004
LZ-3	1	60−140	1.55	140	0.038 ± 0.004
LZ-4	1	90−140	2.16	195	0.033 ± 0.004
LZ-5	1	100−140	3.52	318	0.038 ± 0.006
LZ-6	1	90−140	4.68	422	0.044 ± 0.004
LZ-7	1	120−170	4.71	424	0.043 ± 0.005

where $Q(z)$ and $M(z)$ are the mass and momentum fluxes per unit length, respectively, defined as

$$Q(z) = \int_{-\infty}^{+\infty} \overline{w}(x, z)\, \mathrm{d}x, \tag{12}$$

$$M(z) = \int_{-\infty}^{+\infty} (\overline{w})^2(x, z)\, \mathrm{d}x. \tag{13}$$

In Eq. (10), the limit of $\overline{u}$ when $x \to +\infty$, which quantifies entrainment in the jet, is not known *a priori*. Morton *et al.*[3] avoid the use of this limit through the introduction of a "Top-Hat" entrainment coefficient α_{TH} defined through

$$\frac{\mathrm{d}}{\mathrm{d}z} Q(z) = 2\alpha_{TH} \frac{M}{Q}. \tag{14}$$

The Top-Hat entrainment coefficient has a similar meaning as the Gaussian entrainment coefficient defined above, and is equal to $\sqrt{2\pi}\alpha_G$.

To obtain an explicit expression for the entrainment coefficient, we introduce the conservation of the vertical kinetic energy,[28]

$$\frac{\partial}{\partial z}\left(\frac{1}{2}(\overline{w})^3\right) + \frac{\partial}{\partial x}\left(\frac{1}{2}\overline{u}\,(\overline{w})^2\right) = \frac{\overline{w}}{\rho}\frac{\partial \tau}{\partial x}. \tag{15}$$

The integration of this equation subject to the same boundary conditions as for the integrations (10) and (11), yields

$$\frac{\mathrm{d}}{\mathrm{d}z}\left[\int_{-\infty}^{+\infty} \frac{1}{2}(\overline{w})^3 \mathrm{d}x\right] = \int_{-\infty}^{+\infty} \frac{\partial \overline{w}}{\partial x}\overline{u'w'}\mathrm{d}x. \tag{16}$$

We then introduce the shape functions of the vertical velocity and of the turbulent stress,

$$\overline{w}(x^*, z) = w_m(z) f(x^*, z), \tag{17}$$

$$\tau(x^*, z) = \frac{1}{2}\rho\, w_m(z)^2 j(x^*, z), \tag{18}$$

where $x^* = x/b_w(z)$, with $b_w(z)$ a characteristic length scale of the width of the jet. The integration of the conservation equations using these profiles introduces four dimensionless integrals:

$$I_1 = \int_{-\infty}^{+\infty} f(x^*, z)\,\mathrm{d}x^*, \tag{19}$$

$$I_2 = \int_{-\infty}^{+\infty} f(x^*, z)^2\,\mathrm{d}x^*, \tag{20}$$

$$I_3 = \int_{-\infty}^{+\infty} f(x^*, z)^3\,\mathrm{d}x^*, \tag{21}$$

$$I_4 = \int_{-\infty}^{+\infty} \frac{\partial f(x^*, z)}{\partial x^*} j(x^*, z)\,\mathrm{d}x^*, \tag{22}$$

that are used to write the conservation of the kinetic energy (16) as

$$\frac{\mathrm{d}}{\mathrm{d}z}\left(b_w w_m^3\right) = -\frac{b_w w_m^3}{I_3}\frac{\mathrm{d}I_3}{\mathrm{d}z} - \frac{I_4}{I_3} w_m^3. \tag{23}$$

Combining this equation with Eq. (11), we obtain

$$\frac{\mathrm{d}}{\mathrm{d}z}\left(b_w w_m\right) = 2\left[\frac{\mathcal{C}}{2} + \frac{b_w}{2}\frac{\mathrm{d}\ln\mathcal{A}}{\mathrm{d}z}\right] w_m, \tag{24}$$

which is equivalent to Eq. (2) with

$$\alpha_G \equiv \frac{\mathcal{C}}{2} + \frac{b_w}{2}\frac{\mathrm{d}\ln\mathcal{A}}{\mathrm{d}z}, \tag{25}$$

$$\mathcal{A} = \frac{I_3 I_1}{I_2^2} = \frac{\int_{-\infty}^{+\infty} f(x^*, z)^3\,\mathrm{d}x^* \int_{-\infty}^{+\infty} f(x^*, z)\,\mathrm{d}x^*}{\left(\int_{-\infty}^{+\infty} f(x^*, z)^2\,\mathrm{d}x^*\right)^2}, \tag{26}$$

$$\mathcal{C} = \frac{I_4}{I_3} = \frac{\int_{-\infty}^{+\infty} \frac{\partial f(x^*, z)}{\partial x^*} j(x^*, z)\,\mathrm{d}x^*}{\int_{-\infty}^{+\infty} f(x^*, z)^3\,\mathrm{d}x^*}. \tag{27}$$

The dimensionless parameters $\mathcal{A}$ and $\mathcal{C}$ defined above play a similar role as the parameters A and C introduced by Kaminski *et al.*,[7] but their definition is somewhat different. $\mathcal{A}$ depends only on the shape of the velocity profile, and equals to $\sqrt{4/3}$ for a Gaussian profile. $\mathcal{C}$ can be interpreted as the fraction of kinetic energy driving entrainment. For a Gaussian velocity profile, $\mathcal{C} = \sqrt{3/\pi}\, I_4$, where I_4 is the integral defined in (22) as a function of the Reynolds turbulent shear stress only.

B. Measurements of the Reynolds turbulent shear stress

We compute the Reynolds turbulent shear stress from the fluctuations of the horizontal and vertical velocities, and we fit it by the same type of functions as the one used in Wang and Law,[6]

$$j\left(\frac{x}{z}\right) = c_0\left\{\exp\left[-c_1\left(\frac{x}{z} - c_2\right)^2\right] - \exp\left[-c_1\left(\frac{x}{z} + c_2\right)^2\right]\right\}, \tag{28}$$

where c_0, c_1, and c_2 are fitting parameters.

The values of $\mathcal{C}$, computed from literature data where the Reynolds stress was measured,[18,20,21,23,29] are given in Table III. The comparison between direct measurements and values of α_G predicted from the turbulent shear stress (i.e., $\mathcal{C}/2$) shows a good agreement between the two. However, only data obtained at large Re_0 are considered here.

In our experiments, we did not observe any systematic evolution, within error bars, of the shape of Reynolds turbulent shear stress with z^* or with Re_0. The mean profiles of the turbulent shear stress shown in Figure 5 yields $\mathcal{C}/2 \approx 0.030 \pm 0.005$ which is fully consistent with literature data at high Re_0 (>1500). On the other hand, the value of α_G in our experiments (Figure 6) is in most

TABLE III. Values of the fitting parameters of the profile of the Reynolds turbulent shear stress calculated from literature data and corresponding theoretical and measured α_G (Eq. (25)).

d (mm)	z^*	Re_0	c_0	c_1	c_2	$\mathcal{C}/2$	α_G	References
12.7	5–40	17 800	0.10	60	0.02	0.034 ± 0.003	0.029 ± 0.006	18
12.7	47–155	34 000	0.08	80	0.02	0.032 ± 0.003	0.033 ± 0.003	20
13	65–118	30 000	0.08	80	0.02	0.032 ± 0.004	0.033 ± 0.004	21
5	10–60	1500	0.07	70	0.02	0.029 ± 0.003	0.034 ± 0.006	23
6	45–80	2635–5197	0.1	60	0.02	0.036 ± 0.005	0.036 ± 0.005	29

cases larger than the expected theoretical value of 0.03 (i.e., corresponding to $\mathcal{C}/2$). In the present formalism, this discrepancy implies that additional contributions to entrainment must be taken into account. We thus propose to introduce the second-order contribution of the axial components of the Reynolds stress to entrainment, which can be seen as a "production term" usually neglected.[31]

C. Second-order model of turbulent entrainment

We now write the momentum and kinetic energy equations, with the addition of the axial terms of the Reynolds stress, $\tau_{ax} = -\rho\left(\overline{w'^2} - \overline{u'^2}\right)$,

$$\frac{\partial \overline{u}\,\overline{w}}{\partial x} + \frac{\partial (\overline{w})^2}{\partial z} = \frac{1}{\rho}\left[\frac{\partial}{\partial x}(\tau) + \frac{\partial}{\partial z}(\tau_{ax})\right], \tag{29}$$

$$\frac{\partial}{\partial z}\left(\frac{1}{2}(\overline{w})^3\right) + \frac{\partial}{\partial x}\left(\frac{1}{2}\overline{u}\,(\overline{w})^2\right) = \frac{\overline{w}}{\rho}\left[\frac{\partial}{\partial x}(\tau) + \frac{\partial}{\partial z}(\tau_{ax})\right]. \tag{30}$$

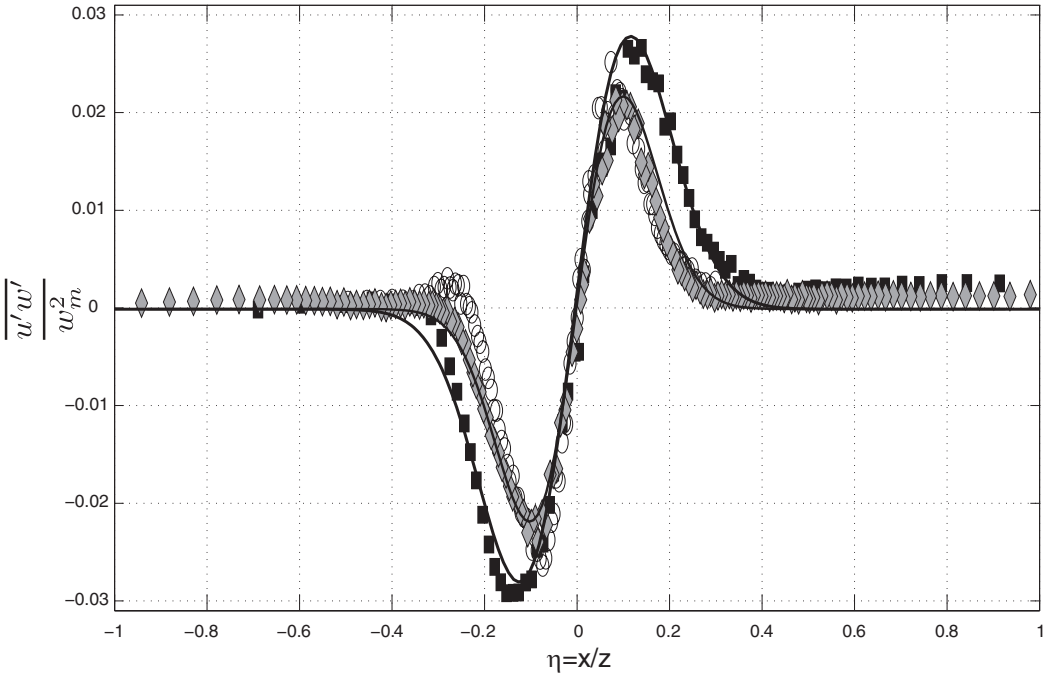

FIG. 5. Average profiles of the turbulent Reynolds shear stress obtained for three experiments: HZ-3 (black squares), IZ-3 (gray diamonds), and LZ-2 (white circles).

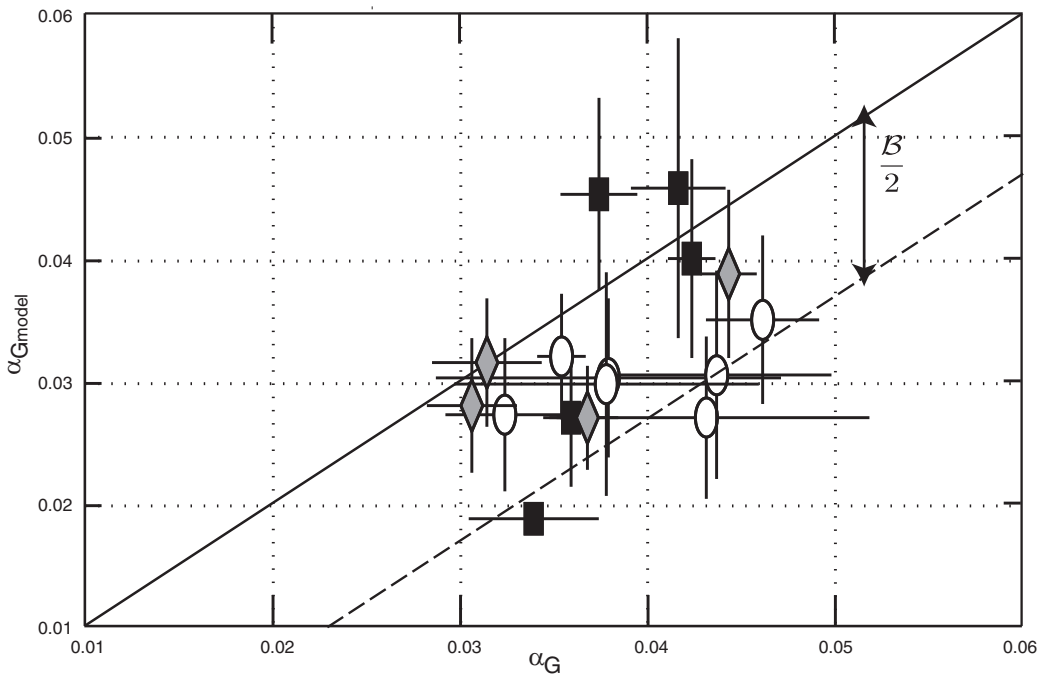

FIG. 6. Comparison between model predictions ($\alpha_{G_{model}} = \frac{\mathcal{C}}{2}$) and measured α_G at small (white circles), intermediate (gray diamonds), and large distances from the source (black squares). The thick black line corresponds to model predictions without the second order contribution to entrainment, and the dashed line corresponds to the complete model (Eq. (35)) with the average contribution of the axial component of the Reynolds stress, $\frac{\mathcal{B}}{2} = 0.013$.

The integration of these two equations subject to the same boundary conditions as in Sec. III A yields

$$\frac{\mathrm{d}}{\mathrm{d}z}\left(b_w w_m^2\right) = \frac{b_w w_m^2}{(I_2 + J_1)} \frac{\mathrm{d}(I_2 + J_1)}{\mathrm{d}z}, \tag{31}$$

$$\frac{\mathrm{d}}{\mathrm{d}z}\left(b_w w_m^3\right) = -\frac{b_w w_m^3}{I_3} \frac{\mathrm{d}I_3}{\mathrm{d}z} - \frac{I_4}{I_3} w_m^3 - \frac{J_2}{I_3} w_m^3, \tag{32}$$

where we have introduced two new integral profiles associated with the axial terms of the Reynolds stress,

$$J_1 = \frac{-1}{\rho} \frac{1}{w_m^2} \int_{-\infty}^{+\infty} \tau_{ax}\, \mathrm{d}x^*, \tag{33}$$

$$J_2 = \frac{-b_w}{\rho d} \frac{1}{w_m^3} \int_{-\infty}^{+\infty} \overline{w} \frac{\partial}{\partial z^*} (\tau_{ax})\, \mathrm{d}x^*. \tag{34}$$

After some algebra, and combining Eqs. (29) and (30), we obtain a new expression for the mass conservation equation, hence for α_G,

$$\frac{\mathrm{d}}{\mathrm{d}z}(b_w w_m) = 2\,\alpha_G\, w_m = 2\left[\frac{\mathcal{C}}{2} + \frac{b_w}{2} \frac{\mathrm{d}\ln \mathcal{A}^*}{\mathrm{d}z} + \frac{\mathcal{B}}{2}\right] w_m, \tag{35}$$

with

$$\mathcal{A}^* = \frac{I_3 I_1}{(I_2 + J_1)^2}, \tag{36}$$

$$\mathcal{B} = \frac{J_2}{I_3}. \tag{37}$$

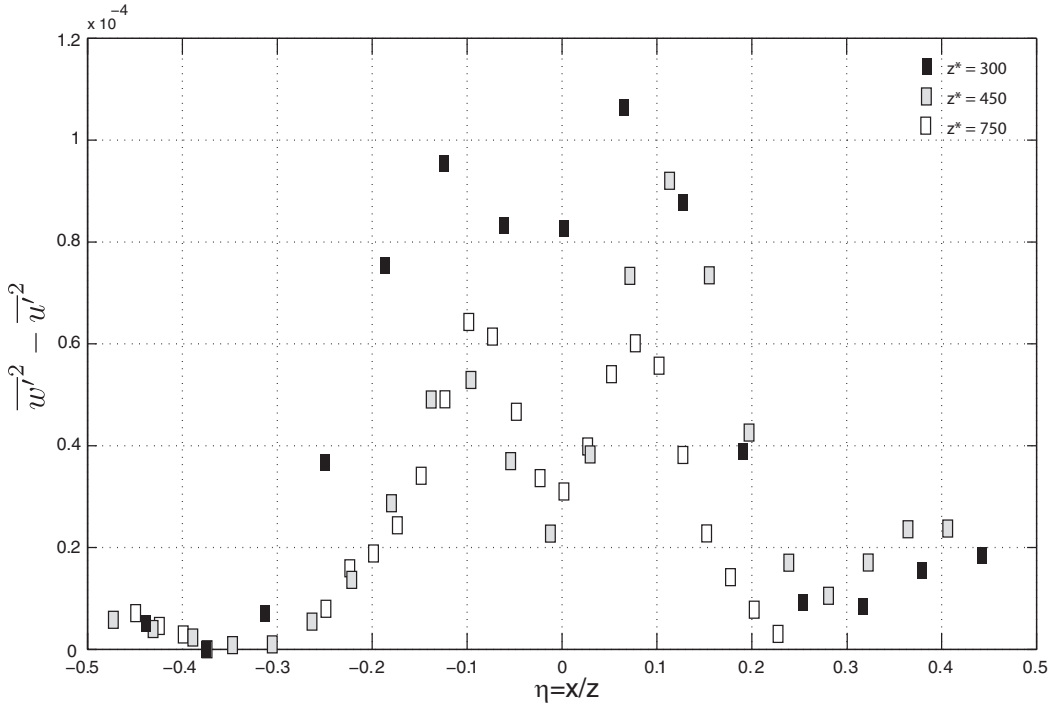

FIG. 7. Measured profiles of τ_{ax} for the experiment HZ-3 ($Re_0 = 139$) at different distances from the source.

We use the experimental profiles to evaluate the order of magnitude of the second-order contributions of the axial terms of the Reynolds stress tensor to entrainment. The first contribution, J_1, scales as $(\overline{w'^2} - \overline{u'^2})/w_m^2$ and is of order 10^{-1}, thus can be neglected compared to I_2 which is of order unity, hence $\mathcal{A}^* \approx \sqrt{4/3}$.

We evaluate the order of magnitude of the second contribution J_2 using the following scaling:

$$J_2 \sim 4\alpha_G \frac{b_w^2}{M_\infty} \frac{\partial\, \tau_{ax_m}}{\partial z^*}, \tag{38}$$

where τ_{ax_m} is the value of τ_{ax} at $x = 0$, obtained from the evolution of the axial terms of the Reynolds stress with z^*, illustrated in Figure 7. The average resulting contribution of the axial terms of the Reynolds stress, $\mathcal{B}/2 \equiv J_2/2I_3$ is ≈0.013. As illustrated in Figure 6 this contribution is large enough to account for the difference between measured α_G and previous estimates based on "classical" Reynolds shear stress (i.e., $\mathcal{C}/2$). Furthermore, we find that the contribution to entrainment of the axial terms ranges between 0 and 0.012 for HZ and IZ experiments and can be up to 0.026 for LZ experiments. This result can be taken as an indication that the flow tends to be fully self-similar (i.e., $\mathcal{B}/2$ tends to 0) when the distance from the source increases. However, the evolution to self-similarity appears too slow at low Re_0 (<500) for this contribution to be neglected in our experiments, even at the largest distance from the source. This result is in line with those obtained by Deo *et al.*[32] at Re_0 > 1500 where they stated that Re_0 is a key parameter for the development of the turbulence and that the self-similarity is achieved further when Re_0 decreases.

IV. CONCLUSIONS

Our experimental study of turbulent entrainment in planar jets at small source Reynolds number shows that the entrainment coefficient α_G cannot be described by a single value. A significant variability is observed at small and at large distances from the source, and no systematic evolution is observed as a function of Re_0. We show that this variability can be quantitatively interpreted as the contribution to turbulent entrainment of the axial terms of the Reynolds stress. This contribution is expected to be zero in fully self-similar jets at high, as the ones corresponding to $Re_0 > 1500$, where

the entrainment coefficient can be considered constant with a value $\alpha_G = \mathcal{C}/2 = 0.030 \pm 0.005$. At low Re_0 the development of self-similarity is too small for such a regime to be observed, even at large distances from the source. The question put forward by George[33] about the influence of source conditions on the self-similarity of axisymmetric jets seems them to be quite relevant in planar turbulent jets.

ACKNOWLEDGMENTS

The authors thank two anonymous referees for their constructive comments and Prof. John Kim for his editorial handling of the manuscript. The experimental device was built by Yves Gamblin and Ramon Vazquez-Paseiro at the IPGP workshop. We thank Angela Limare for her constant help in the experiments.

[1] G. Carazzo, E. Kaminski, and S. Tait, "On the dynamics of volcanic columns: A comparison of field data with a new model of negatively buoyant jets," J. Volcanol. Geoth. Res. **178**(1), 94–103 (2008).
[2] A. W. Woods, "Turbulent plumes in nature," Annu. Rev. Fluid Mech. **42**, 391–412 (2010).
[3] B. R. Morton, G. Taylor, and J. S. Turner, "Turbulent gravitational convection from maintained and instantaneous sources," Proc. R. Soc. London, Ser. A **234**, 1–23 (1956).
[4] J. S. Turner, "Turbulent entrainment: The development of the entrainment assumption, and its application to geophysical flows," J. Fluid Mech. **173**, 431–471 (1986).
[5] P. N. Papanicolaou and E. J. List, "Investigations of round turbulent buoyant jets," J. Fluid Mech. **195**, 341–391 (1988).
[6] H. Wang and A. W.-K. Law, "Second-order integral model for a round turbulent buoyant jet," J. Fluid Mech. **459**, 397–428 (2002).
[7] E. Kaminski, S. Tait, and G. Carazzo, "Turbulent entrainment in jets with arbitrary buoyancy," J. Fluid Mech. **526**, 361–376 (2005).
[8] G. Carazzo, E. Kaminski, and S. Tait, "The route of self-similarity in turbulent jets and plumes," J. Fluid Mech. **547**, 137–148 (2006).
[9] G. Carazzo, E. Kaminski, and S. Tait, "On the rise of turbulent plumes: Quantitative effects of variable entrainment for submarine hydrothermal vents, terrestrial and extra terrestrial explosive volcanism," J. Geophys. Res. **113**, B09201, doi:10.1029/2007JB005458 (2008).
[10] G. Carazzo, E. Kaminski, and S. Tait, "The rise and fall of turbulent fountains: a new model for improved quantitative predictions," J. Fluid Mech. **657**, 265–284 (2010).
[11] A. Geyer, J. C. Phillips, and M. Mier-Torrecilla, "Flow behaviour of negatively buoyant jets in immiscible ambient fluid," Exp. Fluids **52**(1), 261–271 (2012).
[12] S. S. Cardoso and S. T. McHugh, "Turbulentplumes with heterogeneous chemical reaction on the surface of small buoyant droplets," J. Fluid Mech. **642**, 49–77 (2010).
[13] R. B. Stothers, "Turbulent atmospheric plumes above line sources with an application to volcanic fissure eruption on the terrestrial planets," J. Atmos. Sci. **46**(17), 2662–2670 (1989).
[14] A. W. Woods, "A model of the plumes above basaltic fissure eruptions," Geophys. Res. Lett. **20**, 1115–1118, doi:10.1029/93GL01215 (1993).
[15] L. S. Glaze, S. M. Baloga, and J. Wimert, "Explosive volcanic eruptions from linear vents on Earth, Venus, and Mars: Comparisons with circular vent eruptions," J. Geophys. Res. **116**, E01011, doi:10.1029/2010JE003577 (2011).
[16] J. C. Rowland, M. T. Stacey, and W. E. Dietrich, "Turbulent characteristics of a shallow wall-bounded plane jet: experimental implications for river mouth hydrodynamics," J. Fluid Mech. **627**, 423–449 (2009).
[17] H. B. Fischer, E. J. List, R. C. Y. Koh, J. Imberger, and N. H. Brooks, "Mixing in inland and coastal waters," *Turbulent Jets and Plumes* (Academic Press, 1979), pp. 315–389, Chap. 9.
[18] D. R. Miller and E. W. Comings, "Static pressure distribution in the free turbulent jet," J. Fluid Mech. **3**(1), 1–16 (1957).
[19] L. J. S. Bradbury, "The structure of a self-preserving turbulent plane jet," J. Fluid Mech. **23**(1), 31 (1965).
[20] G. Heskestad, "Hot-wire measurements in a plane turbulent jet," J. Appl. Mech. **32**, 721–734 (1965).
[21] E. Gutmark and I. Wygnanski, "The planar turbulent jet," J. Fluid Mech. **73**(part 3), 465–495 (1976).
[22] N. E. Kotsovinos, "A study of the entrainment and turbulence in a plane buoyant jet," Ph.D. thesis (California Institute of Technology, 1975).
[23] B. R. Ramaprian and M. S. Chandrasekhara, "LDA measurements in plane turbulent jets," J. Fluid. Eng.-Trans. ASME **107**, 264–271 (1985).
[24] N. E. Kotsovinos, "A note on the spreading rate and virtual origin of a plane turbulent jet," J. Fluid Mech. **77**(2), 305–311 (1976).
[25] I. Namer and M. V. Ötüngen, "Velocity measurements in a plane turbulent air jet at moderate Reynolds numbers," Exp. Fluids **6**, 387–399 (1988).
[26] P. R. Suresh, K. Srinivasan, T. Sundararajan, and S. K. Das, "Reynolds number dependence of plane jet development in the transitional regime," Phys. Fluids **20**, 044105 (2008).
[27] R. C. Deo, "Experimental investigations of the influence of Reynolds number and boundary conditions on a plane air jet," Ph.D. thesis (School of Mechanical Engineering, The University of Adelaide, 2005).
[28] C. H. B. Priestley and F. K. Ball, "Continuous convection from an isolated source of heat," Q. J. R. Meteorol. Soc. **81**, 144–157 (1955).

[29] J. Andreopoulos, A. Praturi, and W. Rodi, "Experiments on vertical buoyant jets in shallow water," J. Fluid Mech. **168**, 305–336 (1986).
[30] R. C. Deo, J. Mi, and G. J. Nathan, "The influence of Reynolds number on a plane jet," Phys. Fluids **20**, 075108 (2008).
[31] S. B. Pope, *Turbulent Flows* (Cambridge University Press, 2000).
[32] R. C. Deo, G. J. Nathan, and J. Mi, "Similarity analysis of the momentum field of a subsonic, plane air jet with varying jet-exit and local Reynolds similarity analysis of the momentum field of a subsonic, plane air jet with varying jet-exit and local Reynolds numbers," Phys. Fluids **25**, 015115 (2013).
[33] W. K. George, "The self-preservation of turbulent flows and its relation to initial conditions and coherent structures," *Advances in Turbulence* (Springer-Verlag, 1989), pp. 39–72.